

---

---

# Quantitative Analysis of <sup>18</sup>F-PF-06684511, a Novel PET Radioligand for Selective $\beta$ -Secretase 1 Imaging, in Nonhuman Primate Brain

Akihiro Takano<sup>1</sup>, Laigao Chen<sup>2</sup>, Sangram Nag<sup>1</sup>, Michael A. Brodney<sup>2</sup>, Ryosuke Arakawa<sup>1</sup>, Cheng Chang<sup>3</sup>, Nahid Amini<sup>1</sup>, Shawn D. Doran<sup>3</sup>, Jason K. Dutra<sup>3</sup>, Timothy J. McCarthy<sup>2</sup>, Charles E. Nolan<sup>2</sup>, Brian T. O'Neill<sup>3</sup>, Anabella Villalobos<sup>3</sup>, Lei Zhang<sup>2</sup>, and Christer Halldin<sup>1</sup>

<sup>1</sup>Department of Clinical Neuroscience, Centre for Psychiatry Research, Karolinska Institutet and Stockholm County Council, Stockholm, Sweden; <sup>2</sup>Worldwide Research and Development, Pfizer Inc., Cambridge, Massachusetts; and <sup>3</sup>Worldwide Research and Development, Pfizer Inc., Groton, Connecticut

$\beta$ -secretase 1 (BACE1) is a key enzyme in the generation of  $\beta$ -amyloid, which is accumulated in the brain of Alzheimer disease patients. PF-06684511 was identified as a candidate PET ligand for imaging BACE1 in the brain and showed high specific binding in an initial assessment in a nonhuman primate (NHP) PET study using <sup>18</sup>F-PF-06684511. In this effort, we aimed to quantitatively evaluate the regional brain distribution of <sup>18</sup>F-PF-06684511 in NHPs under baseline and blocking conditions and to assess the target occupancy of BACE1 inhibitors. In addition, NHP whole-body PET measurements were performed to estimate the effective radiation dose.

**Methods:** Initial brain PET measurements were performed at baseline and after oral administration of 5 mg/kg of LY2886721, a BACE1 inhibitor, in 2 cynomolgus monkeys. Kinetic analysis was performed with the radiometabolite-corrected plasma input function. In addition, a wide dose range of another BACE1 inhibitor, PF-06663195, was examined to investigate the relationship between the brain target occupancy and plasma concentration of the drug. Finally, the effective radiation dose of <sup>18</sup>F-PF-06684511 was estimated on the basis of the whole-body PET measurements in NHPs. **Results:** Radiolabeling was accomplished successfully with an incorporation radiochemical yield of 4%–12% (decay-corrected) from <sup>18</sup>F ion. The radiochemical purity was greater than 99%. The whole-brain uptake of <sup>18</sup>F-PF-06684511 peaked (~220% SUV) at approximately 20 min and decreased thereafter (~100% SUV at 180 min). A 2-tissue-compartment model described the time–activity curves well. Pretreatment with LY2886721 reduced the total distribution volume of <sup>18</sup>F-PF-06684511 by 48%–80% depending on the brain region, confirming its *in vivo* specificity. BACE1 occupancy of PF-06663195, estimated using the Lassen occupancy plot, showed a dose-dependent increase. The effective dose of <sup>18</sup>F-PF-06684511 was 0.043 mSv/MBq for humans. **Conclusion:** <sup>18</sup>F-PF-06684511 is the first successful PET radioligand for BACE1 brain imaging that demonstrates favorable *in vivo* binding and brain kinetics in NHPs.

**Key Words:** BACE; PET; Alzheimer disease; nonhuman primate

**J Nucl Med 2019; 60:992–997**

DOI: 10.2967/jnumed.118.217372

**A**lzheimer disease (AD) is the most common dementing disease in the elderly, characterized by extracellular accumulation of toxic  $\beta$ -amyloid peptide (A $\beta$ ) and intraneuronal neurofibrillary tau tangles in the brain (1). A $\beta$  is produced by sequential  $\beta$ - and  $\gamma$ -secretase-mediated cleavage of the amyloid precursor protein.  $\beta$ -secretase 1 (BACE1) is thought to be a key enzyme for A $\beta$  accumulation (2). In postmortem studies, messenger RNA and protein levels of BACE1 were reported to be increased in AD patients in comparison to normal-cognition controls (3–5). Recent amyloid PET imaging studies indicate that amyloid deposit starts 10–20 y before the onset of the disease, which suggests that A $\beta$  accumulation in the brain plays an important role in the early stage of AD pathogenesis (6). Because BACE1-mediated cleavage of amyloid precursor protein is one of the key processes in A $\beta$  accumulation, inhibition of BACE1 is expected to have therapeutic potential for treating AD. In amyloid precursor protein transgenic mice, BACE1 inhibitors have been shown to significantly reduce A $\beta$  accumulation (7–10). In recent years, several BACE1 inhibitors have been investigated in clinical trials (11,12). Measurement of A $\beta$  concentration in cerebrospinal fluid and amyloid imaging have helped to prove the mechanism of action of the drugs. PET radioligands specifically binding to BACE1 may help the evaluation of target engagement and dose selection in clinical trials of BACE1 inhibitors by directly measuring *in vivo* target occupancy. In addition, BACE1 expression levels in AD patients measured by a BACE1-selective PET radioligand may potentially be applied to select the appropriate disease subpopulation for clinical assessment of BACE1 inhibitors.

PF-06684511 has been identified and evaluated as a novel candidate PET ligand that binds to the BACE1 target (half-maximal inhibitory concentration, 0.7 nM) (13). On radiolabeling with <sup>18</sup>F, it demonstrated favorable brain uptake and high binding specificity in nonhuman primates (NHPs) with PET imaging, suggesting it is a promising PET ligand for imaging BACE1 (13). In this research, 3 studies were performed. First, we quantitatively evaluated the regional brain distribution of <sup>18</sup>F-PF-06684511 in NHPs under baseline and blocking conditions with a BACE1 inhibitor, LY2886721 (14). Second, a wide dose range of another BACE1 inhibitor, PF-06663195 (15), was examined to investigate the relationship between the target occupancy and plasma concentration of the drug. Last, the effective radiation dose of <sup>18</sup>F-PF-06684511 was estimated on the basis of the NHP whole-body PET measurements.

---

Received Jul. 10, 2018; revision accepted Nov. 26, 2018.  
For correspondence or reprints contact: Akihiro Takano, Department of Clinical Neuroscience, Karolinska Institutet, Stockholm, Sweden S-171 76.  
E-mail: akihiro.takano@ki.se  
Published online Dec. 7, 2018.  
COPYRIGHT © 2019 by the Society of Nuclear Medicine and Molecular Imaging.

## MATERIALS AND METHODS

### Radioligand Synthesis

<sup>18</sup>F-PF-06684511 was synthesized as reported previously (13).

### Subjects

Seven cynomolgus monkeys (2 female, 5 male; body weight, 3,725–9,700 g) were used in this research. Two NHPs (1 female [NHP1], 1 male [NHP2]) were used in the baseline/blocking study. Four NHPs (2 female [NHP1 and NHP3], 2 male [NHP4 and NHP5]) were used in the target occupancy study, with 1 female NHP (NHP1) used in both studies. Two male NHPs (NHP6 and NHP7) were used in the whole-body dosimetry study.

The NHPs were housed in the Astrid Fagraeus Laboratory of the Swedish Institute for Infectious Disease Control, Solna, Sweden. All studies were approved by the Animal Ethics Committee of the Swedish Animal Welfare Agency (N185/14) and performed according to “Guidelines for Planning, Conducting and Documenting Experimental Research” (Dnr 4820/06–600) of Karolinska Institutet.

### Brain PET System

Brain PET measurements were conducted using a High Resolution Research Tomograph (Siemens Molecular Imaging). List-mode data were reconstructed using the ordinary Poisson 3-dimensional ordered-subset expectation maximization algorithm.

### Drug Administration

LY2886721 was used in the baseline–blocking study. It was administered orally (via gavage) approximately 2 h before PET scanning, at a dose of 5 mg/kg and a dosing volume of 2 mL/kg.

PF-06663195 was used in the target occupancy study. It was administered intravenously as a bolus (1 min, 0.1 mL/kg) followed by a constant infusion (1.0 mL/h/kg) to the end of the scan. The bolus injection was started approximately 10 min before PET scanning. Four different doses (0.022 mg/kg + 0.005 mg/h/kg, 0.089 mg/kg + 0.021 mg/h/kg, 0.133 mg/kg + 0.032 mg/h/kg, and 0.266 mg/kg + 0.064 mg/h/kg) of PF-06663195 were tested in this study. On the basis of our previous experience, the intravenous bolus-plus-infusion dosing method typically results in more reliable and consistent plasma pharmacokinetic exposure than oral dosing in anesthetized NHPs. The intravenous infusion protocol was chosen on the basis of the predicted intravenous bolus-plus-infusion pharmacokinetic profile using a Pfizer internal pharmacokinetic model, making use of data from a previously performed Pfizer pharmacokinetic study with bolus intravenous dosing of PF-06663195 in NHPs.

### Brain PET Measurements

Anesthesia was induced by intramuscular injection of ketamine hydrochloride (~10 mg/kg) and maintained by the administration of a mixture of isoflurane (1.5%–2.0%), oxygen, and medical air with endotracheal intubation.

A transmission scan of 6 min using a single <sup>137</sup>Cs source was performed before the <sup>18</sup>F-PF-06684511 injection. List-mode data were acquired continuously for 180 min (in the baseline–blocking study) and 123 min (in the target occupancy study) immediately after intravenous injection of the radioligand. Images were reconstructed with a series of 28 frames (1 min × 5, 3 min × 5, 6 min × 5, and 10 min × 13) in the baseline–blocking study and with a series of 34 frames (20 s × 9, 1 min × 3, 3 min × 5, and 6 min × 17) in the target occupancy study. Each PET measurement for the same NHP was separated by at least 5 wk. In the baseline–blocking study, 1 baseline and 1 blocking PET measurement were performed for each NHP. In the target occupancy study, 1 baseline and 2 blocking PET measurements were performed per NHP, corresponding to intravenous administration of 2 different doses of PF-06663195.

### Arterial Blood Sampling

An arterial blood sampling system (Allogg AB) at a speed of 3 mL/min was used to measure the continuous radioactivity in the blood for the first 3 min. The dispersion correction was made for the measured radioactivity. Thereafter, blood sampling (1–3 mL/sample) was performed manually for measurement of metabolism and radioactivity at 4, 10, 20, 30, 45, 60, 90, and 120 min (plus 150 and 180 min in baseline–blocking study only).

### Radiometabolite Analysis

A reversed-phase radio–high-performance liquid chromatography method was used to determine the amount of unchanged <sup>18</sup>F-PF-06684511 and its radiometabolites in NHP plasma.

### Protein Binding

The free fraction ( $f_p$ ) of <sup>18</sup>F-PF-06684511 in plasma was estimated using an ultrafiltration method (16).

### Measurement of Plasma Concentration of LY2886721 and PF-06663195

Under the drug pretreatment condition, venous blood samples (1 mL each) were taken at –125 min, –60 min, –1 min, 60 min, 120 min, and 180 min for LY2886721 and at –13 min, –1 min, 30 min, 60 min, 90 min, and 120 min for PF-06663195 when the time of the radioligand injection was time 0. The plasma concentration of LY2886721 and PF-06663195 was measured at a pharmacokinetic analysis lab (Unilabs York Bioanalytical Solutions).

### MRI Measurements

T1-weighted MR images of the individual NHP brains had been obtained using a 1.5-T GE Healthcare Signa system. The MRI sequence was a 3-dimensional spoiled gradient-recalled protocol with the following settings: repetition time, 21 ms; flip angle, 35°; field of view, 12.8 cm; matrix, 256 × 256 × 128; number of slices, 128; slice thickness, 1.0 mm; and number of excitations, 2.

### Brain Image Analysis

The image data, including kinetic model analysis, were analyzed using PMOD, version 3.4 (PMOD Technologies LLC). The volumes of interest were delineated manually on the MR images of each NHP for the whole brain and for 13 brain regions: cerebellum, anterior cingulate cortex, frontal cortex, temporal cortex, caudate, putamen, thalamus, occipital cortex, parietal cortex, amygdala, hippocampus, insular cortex, and ventral striatum. The summed PET images of all frames were coregistered to the MR image of the same NHP (Supplemental Fig. 1; supplemental materials are available at <http://jnm.snmjournals.org>). The coregistration parameters were applied to the dynamic PET data to generate the time–activity curves of brain regions for each PET measurement.

### Kinetic Model Analysis

The 1-tissue-compartment model (1TC) and 2-tissue-compartment model (2TC) were evaluated, with the radiometabolite-corrected plasma radioactivity as the input function. Fractional blood volume was set to 5% in all regions. As the main outcome measure, the total distribution volume ( $V_T$ ), defined as  $K_1/k_2$  by 1TC and  $K_1/k_2 \times (1 + k_3/k_4)$  by 2TC, was calculated. The goodness of fit was assessed using Akaike information criteria.

The time stability of  $V_T$  was evaluated by truncating the PET data frame by frame.

### Graphical Analysis

The Logan graphical plot was used to estimate  $V_T$  (17) for the baseline–blocking study.  $T^*$  was determined on the basis of the model function in PMOD software, where the earliest sample time point of  $t^*$  was searched so that the deviation between the regression and all

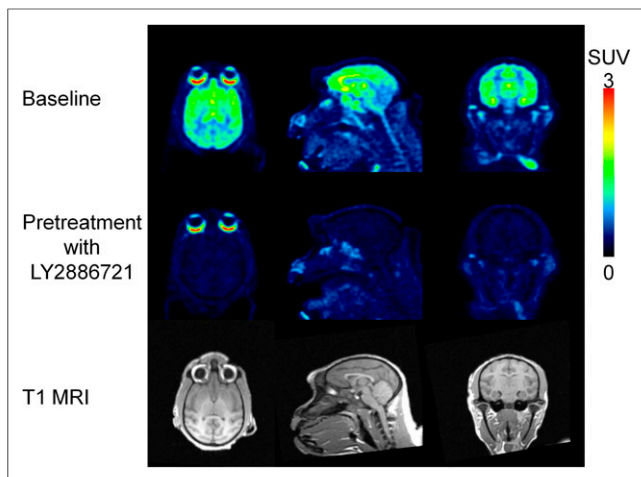


**FIGURE 1.** PET images of  $^{18}\text{F}$ -PF-06684511 summed from 90 min to 180 min at baseline and under pretreatment with LY2886721 and corresponding MR image in NHP1.

measurements was less than 10%.  $T^*$  was 4–20 min in the baseline-blocking study.

To evaluate the correlation between  $V_T$  values estimated from 2TC and Logan graphical analysis, the  $V_T$  values of 4 baseline PET measurements for the occupancy study were also calculated.

#### Estimation of Target Occupancy

Because there was no expected reference region, the target occupancy was estimated by the Lassen occupancy plot (18,19) using  $V_T$  calculated by 2TC. The 13 brain regions were included in the plot.

#### Relationship Between BACE1 Occupancy and PF-06663195

The average plasma concentration was determined by area under the curve using the trapezoidal rule during a 120-min PET scan of PF-06663195. The relationship between average plasma concentration and the BACE1 occupancy in the brain was estimated by an  $E_{\text{max}}$  model, which is a single-binding-site model, with the following equation:  $\text{occupancy (\%)} = C / (EC_{50} + C) \times E_{\text{max}}$ , where  $C$  is the plasma

concentration of PF-06663195,  $EC_{50}$  is the plasma concentration required to achieve 50% of the maximum occupancy, and  $E_{\text{max}}$  is the maximum occupancy. In this analysis,  $E_{\text{max}}$  was set as 100%. Similarly,  $ED_{50}$  for the total dose was estimated.

#### Whole-Body PET System

Whole-body PET measurements were conducted using a Biograph TruePoint TrueV PET/CT system (Siemens Medical Solutions).

#### Whole-Body PET Measurements

Anesthesia was induced by intramuscular injection of ketamine hydrochloride ( $\sim 10$  mg/kg) at Astrid Fagraeus Laboratory and maintained by intravenous infusion of ketamine (4 mg/kg/h) and xylazine (0.4 mg/kg/h) with a pump. Before the PET scan, a whole-body low-dose CT scan was obtained for attenuation correction. After intravenous bolus injection of  $^{18}\text{F}$ -PF-06684511, a whole-body PET scan was performed for approximately 180 min.

#### Image Analysis of the Whole-Body PET

Volumes of interest were drawn on high-uptake organs such as the brain, lung, heart, kidney, spleen, pancreas, liver, gallbladder, stomach, urinary bladder, small intestine, bone (lumbar vertebrae), and esophagus (for only 1 NHP) with the help of the CT images for anatomic landmarks. The absorbed radiation dose in humans was estimated with OLINDA/EXM 1.1 software, using the adult male (70-kg) reference model (20).

## RESULTS

#### Radioligand Synthesis

$^{18}\text{F}$ -PF-06684511 was successfully radiosynthesized within 80–95 min from the end of beam. Radiochemical purity was more than 99%, and radiochemical yield was 4%–12%.  $^{18}\text{F}$ -PF-06684511 was stable for 2 h after the end of synthesis.

#### PET Data in the Baseline-Blocking Study

The mean injected radioactivity ( $n = 4$ ) of  $^{18}\text{F}$ -PF-06684511 was  $149 \pm 22$  MBq (range, 117–168 MBq). The mean regional activity at the time of injection was  $103 \pm 49$  GBq/ $\mu\text{mol}$  (range, 73–175 GBq/ $\mu\text{mol}$ ), and the mean injected mass was  $0.7 \pm 0.3$   $\mu\text{g}$  (range, 0.3–1.0  $\mu\text{g}$ ). The summed PET images at baseline and under drug treatment are shown in Figure 1. Brain uptake decreased after LY2886721 administration (5 mg/kg, orally). Time-activity curves of the whole brain peaked ( $\sim 220\%$  SUV on average) at approximately 20 min and thereafter decreased ( $\sim 100\%$  SUV at 180 min on average) at baseline, and the time at the peak became earlier under the pretreatment condition (Supplemental Fig. 2). Regional time-activity curves of NHP1 are shown in Figure 2. Uptake was relatively higher in subcortical regions than in cortical regions. The washout from the peak was faster in the cerebellum than in other regions. Uptake decreased in all brain regions after the administration of LY2886721. The average time-activity curves at baseline for the 180-min PET data ( $n = 2$ ) and the 120-min PET data ( $n = 4$ ) are shown in Supplemental Figures 3A and 3B.

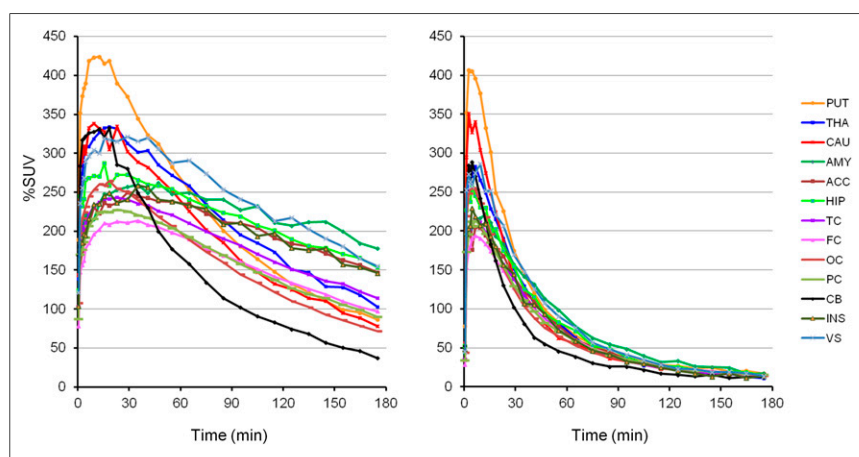


**FIGURE 2.** Regional brain time-activity curves of  $^{18}\text{F}$ -PF-06684511 at baseline (left) and under pretreatment with LY2886721 (right) in NHP1. PUT = putamen; THA = thalamus; CAU = caudate; AMY = amygdala; ACC = anterior cingulate cortex; HIP = hippocampus; TC = temporal cortex; FC = frontal cortex; OC = occipital cortex; PC = parietal cortex; CB = cerebellum; INS = insular cortex; VS = ventral striatum.

#### Radioligand in Plasma

Approximately 40% of  $^{18}\text{F}$ -PF-06684511 remained unmetabolized in the plasma of

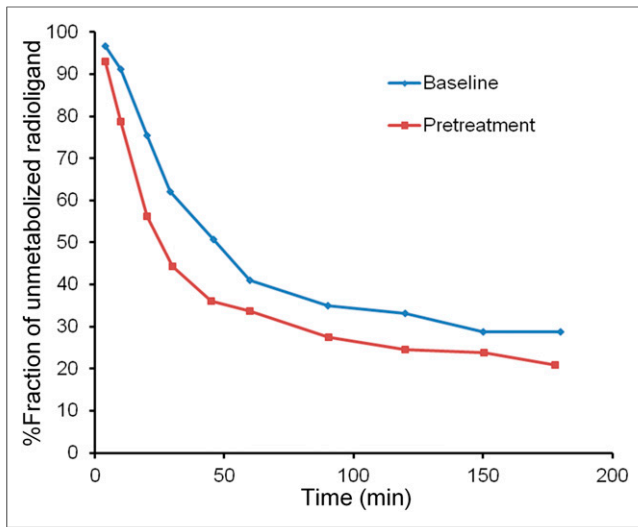


**FIGURE 3.** Percentage fraction of unmetabolized  $^{18}\text{F}$ -PF-06684511 in plasma in NHP 1.

NHP1 at 90 min (Fig. 3). There were no radiometabolites showing higher lipophilicity than  $^{18}\text{F}$ -PF-06684511 (Supplemental Fig. 4). The average fraction of the unchanged radioligand for the baseline–blocking study and the occupancy study is shown in Supplemental Figure 5. The plasma free fraction was 23.4% and 18.8% at baseline and 22.4% and 29.2% at pretreatment in NHP1 and NHP2, respectively.

#### Kinetic Analysis and Target Occupancy of LY2886721

In most regions, both 1TC and 2TC described the time–activity curves well, whereas the description was better with 2TC in some regions such as the hippocampus (Fig. 4). When the first 2 NHPs’ baseline data were combined, 18 of 26 brain regions showed a better fit with 2TC for Akaike information criteria. Estimated kinetic parameters and  $V_T$  are shown in Supplemental Table 1 for 1TC and Supplemental Table 2 for 2TC.  $V_T$  values correlated well between 1TC and 2TC ( $R^2 > 0.99$ ). Individual  $V_T$  values estimated by 2TC are shown in Supplemental Figure 6.  $V_T$  decreased in all brain regions after administration of LY2886721 (48%–80%). Lassen occupancy plots are shown in Supplemental Figure 7. The estimated occupancy after LY2886721 pretreatment

was 91.6% and 92.1% for NHP1 and NHP2, respectively.  $V_{\text{ND}}$  was estimated to be 2.7 and 3.1 for NHP1 and NHP2, respectively.

#### Time Stability of Estimated $V_T$

The percentage change in  $V_T$  from that calculated using 180-min data is shown in Supplemental Figure 8. The 120-min data showed less than a 10% change in all investigated brain regions and less than 5% in most brain regions.

#### Graphical Analysis

Examples of Logan graphical plots are shown in Supplemental Figure 9.  $V_T$  values estimated by Logan graphical plots are shown in Supplemental Table 3. The correlation between  $V_T$  estimated by Logan graphical plots and 2TC is shown in Supplemental Figure 10. When a linear regression without an intercept was made, the regression equation was expressed as  $y = 0.9376x$  ( $R^2$  was 0.99).  $V_T$  values estimated with Logan plots were negatively biased by approximately 6%, compared with those estimated with 2TC.

#### PET Data in the Target Occupancy Study

The mean injected radioactivity ( $n = 12$ ) of  $^{18}\text{F}$ -PF-06684511 was  $156 \pm 6$  MBq (range, 143–165 MBq). The mean molar activity at the time of injection was  $69 \pm 32$  GBq/ $\mu\text{mol}$  (range, 32–133 GBq/ $\mu\text{mol}$ ), and the mean injected mass was  $1.2 \pm 0.5$   $\mu\text{g}$  (range, 0.5–2.1  $\mu\text{g}$ ). The uptake of  $^{18}\text{F}$ -PF-06684511 decreased in all brain regions with administration of PF-06663195. The target occupancies estimated using Lassen occupancy plots with  $V_T$  were 39.5%–98.1% (examples are shown in Supplemental Fig. 11). Estimated  $V_{\text{ND}}$  was  $3.72 \pm 0.87$  (range, 2.70–5.24). The time courses of the plasma concentration of PF-06663195 are shown in Supplemental Figure 12. The exposure–occupancy curve was well fitted with an  $E_{\text{max}}$  model.  $\text{EC}_{50}$  was estimated to be 3.75 ng/mL (Fig. 5).  $\text{ED}_{50}$  was estimated to be 0.049 mg/kg (Supplemental Fig. 13).

#### Whole-Body PET

The injected radioactivity of  $^{18}\text{F}$ -PF-06684511 was 219 and 200 MBq, respectively. The molar activity at the time of injection was 30 and 32 GBq/ $\mu\text{mol}$ , respectively, and the injected mass was 3.2 and 2.7  $\mu\text{g}$ , respectively. The highest average uptake (percentage injected dose) was found in the stomach ( $\sim 34\%$  at 175 min), followed by the liver ( $\sim 18\%$  at around 11 min) (Fig. 6). The radioligand was excreted partly via the bile and gastrointestinal

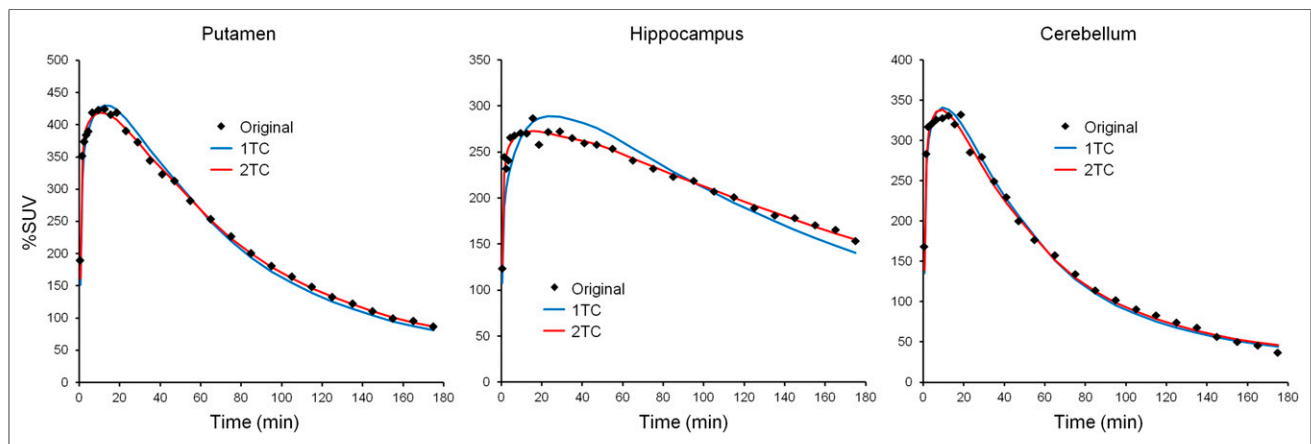


**FIGURE 4.** Typical compartmental-model curve fitting of  $^{18}\text{F}$ -PF-06684511. Data are from baseline PET of NHP1.

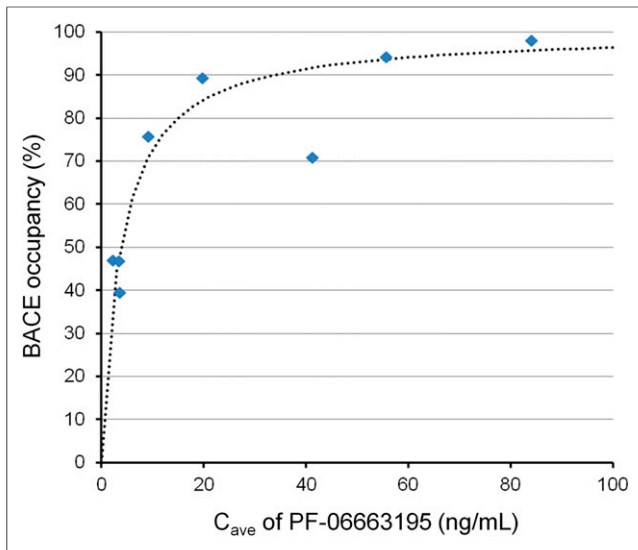


**FIGURE 5.** Relationship between BACE1 occupancy and PF-06663195 average plasma concentration ( $C_{ave}$ )

tract and partly via the urinary tract (Fig. 6; Supplemental Fig. 14). The numbers of disintegrations in the source organs are shown in Supplemental Table 4. The largest absorbed dose was in the stomach wall (0.22 mSv/MBq) (Supplemental Table 5). The calculated human whole-body effective dose was about 0.043 mSv/MBq (Supplemental Table 5).

## DISCUSSION

A novel PET radioligand for BACE1,  $^{18}\text{F}$ -PF-06684511, was evaluated in NHPs and showed favorable characteristics as a PET radioligand, with high brain uptake and high specific binding in the present study. Development of PET radioligands for BACE1 was attempted previously.  $^{11}\text{C}$ -Me-NCFB was developed, but no evaluation using PET imaging was performed (21). Further study using the radioligand has not been reported so far.  $^{11}\text{C}$ -BSI-IV was also reported to be a potential PET radioligand for BACE1, but low uptake in rodents and a low degree of specific binding led to limited use (22).

In this study,  $V_T$  estimated using 2TC showed regional differences, with cerebellum being the lowest (23), and this regionality

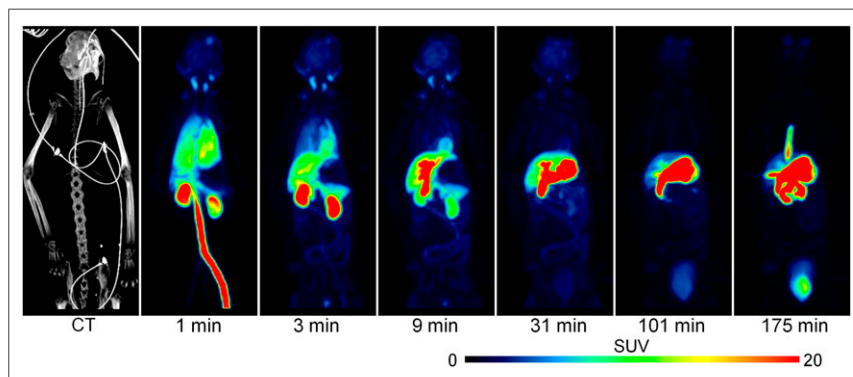


**FIGURE 6.** Whole-body PET images of  $^{18}\text{F}$ -PF-06684511 in NHP7. Images are maximum-intensity projection.

corresponded to the distribution of BACE1 in the brain. No reference region was identified, because the estimated  $V_T$  values in all brain regions evaluated, including cerebellum, decreased after the administration of a BACE1 inhibitor. As an exploratory evaluation, the white matter was also investigated as a potential reference region, but uptake in the white matter decreased after the administration of a BACE1 inhibitor (Supplemental Figs. 15A and 15B). The estimated  $V_{ND}$  from Lassen plots was approximately 3, whereas the  $V_T$  values ranged from 6 to 18. The ratios of specific-to-nonspecific binding were in the range of 1–6. This means that about 50%–86% of  $V_T$  was specific, depending on brain region.

The time stability of  $V_T$  values showed that most of the investigated brain regions had less than a 5% change from 180 min to 120 min. This stability was considered to be sufficient to perform 120-min PET measurements for  $^{18}\text{F}$ -PF-06684511 in NHPs.

In the radio-high-performance liquid chromatography analysis, there were no radiometabolites showing higher lipophilicity than  $^{18}\text{F}$ -PF-06684511. Although the results could not completely exclude the possibility of brain-permeable radiometabolites, the impact of radiometabolites on the quantitative analysis was thought to be low because the PET data were well described by 1TC and 2TC models using the metabolite-corrected plasma as the input function. The goodness of fit was assessed for the blocking data of the first 2 NHPs with LY2886721, by which the binding of  $^{18}\text{F}$ -PF-06684511 was almost fully blocked. Akaike information criteria showed a better fit with 1TC than 2TC in 21 of 26 time-activity curves. This finding may indicate a lower likelihood that radiometabolites were entering the brain, which would contribute to the second tissue compartment. The time stability of  $V_T$  in the blocking study (Supplemental Fig. 16) supports the hypothesis that radiometabolites contributed only minimally to quantification of radioligand uptake in the brain, since truncation of the dynamic scan data did not lead to significant bias in any brain regions.

BACE1 inhibition has been one of the active targets for drug development for AD (24,25). Clinical development of several BACE1 inhibitors such as E2609 (NCT03036280 and NCT02956486), LY3202626 (NCT03367403), and CNP520 (NCT03131453 and NCT02565511) are still active, whereas clinical trials of some other BACE inhibitors, such as MK-8931 (NCT01739348 and NCT01953601) and lanabecestat (NCT02245737), were terminated because of insufficient efficacy. So far, the clinical trials of BACE1 inhibitors have not shown the promising results initially expected (24,25). Timing of drug administration in the

disease progress, patient selection, and target engagement of the drugs may be potential factors contributing to the failure (24,25). BACE1 was reported to regulate neurogenesis in early developmental stages (26). A recent report showed that BACE1 regulates adult hippocampal neurogenesis and that complete inhibition of BACE1 activity dysregulates adult hippocampal neurogenesis but partial inhibition would not impact it (27). Therefore, partial inhibition of BACE1 activity was proposed as a more suitable therapeutic approach. The balance between the  $\text{A}\beta$  depletion and adult hippocampal neurogenesis may be an important factor to improve the development strategy of BACE1 inhibitors. In this study,  $^{18}\text{F}$ -PF-06684511 showed high dynamic range in quantifying

BACE1 binding as demonstrated by dose-dependent occupancy with a BACE1 inhibitor, which allows detection of small changes in BACE1 availability under disease or partial-blockade conditions. Potential application of <sup>18</sup>F-PF-06684511 PET in clinical trials of BACE1 inhibitors may include stratifying AD patients by measuring the BACE1 level in the brain, confirming target engagement of the drugs, and fine-tuning the doses by measuring in vivo occupancy.

Two BACE1 inhibitors, LY2886721 and PF-06663195, used to test the specific binding of <sup>18</sup>F-PF-06684511 to BACE1 in this study, share a fluorophenyl-pyrazine/pyridine-carboxamide substructure. It would be worth examining whether BACE1 inhibitors with different chemotypes compete with <sup>18</sup>F-PF-06684511 for binding sites in BACE1, as such information would clarify the usefulness of <sup>18</sup>F-PF-06684511 in measurement of target engagement in general.

The whole-body radiation dosimetry study showed a relatively high accumulation in the stomach. In NHP7, even the esophagus was visualized in the late phase (Fig. 6). High uptake in the stomach could lead to relatively high effective doses compared with other <sup>18</sup>F radioligands (28). Some of the excretion from the liver to the bile ducts and lower gastrointestinal tract appeared to flow backward to the stomach and esophagus. The backflow may occur partially because the NHPs were lying in the same position during the PET measurement under anesthesia with intravenous ketamine and xylazine. Stomach uptake is likely to be reduced in human subjects because they are awake and can move the whole body during break times.

## CONCLUSION

<sup>18</sup>F-PF-06684511 demonstrated favorable characteristics as a PET radioligand for BACE1 in NHPs, with high brain uptake and clear blocking effects by BACE1 inhibitors. Further evaluation of this radioligand in humans is warranted.

## DISCLOSURE

This work was sponsored by Pfizer Inc. Laigao Chen, Michael A. Brodney, Cheng Chang, Shawn D. Doran, Jason K. Dutra, Timothy J. McCarthy, Charles E. Nolan, Brian T. O'Neill, Anabella Villalobos, and Lei Zhang were employees of Pfizer Inc. when the study was conducted. No other potential conflict of interest relevant to this article was reported.

## ACKNOWLEDGMENTS

We thank all the members of the Karolinska PET group for their assistance with the PET experiments, including special thanks to Kia Hultberg-Lundberg and Jonas Ahlgren for excellent technical assistance. We also thank Dr. Michael Stabin (Vanderbilt University) for helping with calculation of the absorbed radiation dose.

## REFERENCES

- Ballard C, Gauthier S, Corbett A, Brayne C, Aarsland D, Jones E. Alzheimer's disease. *Lancet*. 2011;377:1019–1031.
- Yan R, Vassar R. Targeting the  $\beta$  secretase BACE1 for Alzheimer's disease therapy. *Lancet Neurol*. 2014;13:319–329.
- Fukumoto H, Cheung BS, Hyman BT, Irizarry MC. Beta-secretase protein and activity are increased in the neocortex in Alzheimer disease. *Arch Neurol*. 2002;59:1381–1389.
- Yang LB, Lindholm K, Yan R, et al. Elevated beta-secretase expression and enzymatic activity detected in sporadic Alzheimer disease. *Nat Med*. 2003;9:3–4.

- Li R, Lindholm K, Yang LB, et al. Amyloid beta peptide load is correlated with increased beta-secretase activity in sporadic Alzheimer's disease patients. *Proc Natl Acad Sci USA*. 2004;101:3632–3637.
- Rodriguez-Vicitez E, Saint-Aubert L, Carter SF, et al. Diverging longitudinal changes in astrogliosis and amyloid PET in autosomal dominant Alzheimer's disease. *Brain*. 2016;139:922–936.
- Eketjäll S, Janson J, Jeppsson F, et al. AZ-4217: a high potency BACE inhibitor displaying acute central efficacy in different in vivo models and reduced amyloid deposition in Tg2576 mice. *J Neurosci*. 2013;33:10075–10084.
- Hussain I, Hawkins J, Harrison D, et al. Oral administration of a potent and selective non-peptidic BACE-1 inhibitor decreases beta-cleavage of amyloid precursor protein and amyloid-beta production in vivo. *J Neurochem*. 2007;100:802–809.
- Neumann U, Rueeger H, Machauer R, et al. A novel BACE inhibitor NB-360 shows a superior pharmacological profile and robust reduction of amyloid- $\beta$  and neuroinflammation in APP transgenic mice. *Mol Neurodegener*. 2015;10:44.
- Sankaranarayanan S, Price EA, Wu G, et al. In vivo beta-secretase 1 inhibition leads to brain Abeta lowering and increased alpha-secretase processing of amyloid precursor protein without effect on neuregulin-1. *J Pharmacol Exp Ther*. 2008;324:957–969.
- Vassar R. BACE1 inhibitor drugs in clinical trials for Alzheimer's disease. *Alzheimers Res Ther*. 2014;6:89.
- Yan R. Stepping closer to treating Alzheimer's disease patients with BACE1 inhibitor drugs. *Transl Neurodegener*. 2016;5:13.
- Zhang L, Chen L, Dutra JK, et al. Identification of a novel positron emission tomography (PET) ligand for imaging  $\beta$ -site amyloid precursor protein cleaving enzyme 1 (BACE-1) in brain. *J Med Chem*. 2018;61:3296–3308.
- May PC, Willis BA, Lowe SL, et al. The potent BACE1 inhibitor LY2886721 elicits robust central A $\beta$  pharmacodynamic responses in mice, dogs, and humans. *J Neurosci*. 2015;35:1199–1210.
- Brodney MA, Beck EM, Butler CR, et al. Utilizing structures of CYP2D6 and BACE1 complexes to reduce risk of drug-drug interactions with a novel series of centrally efficacious BACE1 inhibitors. *J Med Chem*. 2015;58:3223–3252.
- Amini N, Nakao R, Schou M, Halldin C. Determination of plasma protein binding of positron emission tomography radioligands by high-performance frontal analysis. *J Pharm Biomed Anal*. 2014;98:140–143.
- Logan J, Fowler JS, Volkow ND, et al. Graphical analysis of reversible radioligand binding from time-activity measurements applied to [<sup>11</sup>C-methyl]-(-)-cocaine PET studies in human subjects. *J Cereb Blood Flow Metab*. 1990;10:740–747.
- Cunningham VJ, Rabiner EA, Slifstein M, Laruelle M, Gunn RN. Measuring drug occupancy in the absence of a reference region: the Lassen plot re-visited. *J Cereb Blood Flow Metab*. 2010;30:46–50.
- Lassen NA, Bartenstein PA, Lammertsma AA, et al. Benzodiazepine receptor quantification in vivo in humans using [<sup>11</sup>C]flumazenil and PET: application of the steady-state principle. *J Cereb Blood Flow Metab*. 1995;15:152–165.
- Stabin MG, Sparks RB, Crowe E. OLINDA/EXM: the second-generation personal computer software for internal dose assessment in nuclear medicine. *J Nucl Med*. 2005;46:1023–1027.
- Kawai T, Kawashima H, Kuge Y, Saji H. Synthesis and evaluation of <sup>11</sup>C-labeled naphthalene derivative as a novel non-peptidergic probe for the  $\beta$ -secretase (BACE1) imaging in Alzheimer's disease brain. *Nucl Med Biol*. 2013;40:705–709.
- Nordeman P, Estrada S, Odell LR, et al. <sup>11</sup>C-labeling of a potent hydroxyethylamine BACE-1 inhibitor and evaluation in vitro and in vivo. *Nucl Med Biol*. 2014;41:536–543.
- Shinohara M, Petersen RC, Dickson DW, Bu G. Brain regional correlation of amyloid- $\beta$  with synapses and apolipoprotein E in non-demented individuals: potential mechanisms underlying regional vulnerability to amyloid- $\beta$  accumulation. *Acta Neuropathol (Berl)*. 2013;125:535–547.
- Evin G. Future therapeutics in Alzheimer's disease: development status of BACE inhibitors. *BioDrugs*. 2016;30:173–194.
- Coimbra JRM, Marques DFF, Baptista SJ, et al. Highlights in BACE1 inhibitors for Alzheimer's disease treatment. *Front Chem*. 2018;6:178.
- Hu X, He W, Luo X, Tsubota KE, Yan R. BACE1 regulates hippocampal astrogliogenesis via the Jagged1-Notch pathway. *Cell Reports*. 2013;4:40–49.
- Chatila ZK, Kim E, Berlé C, et al. BACE1 regulates proliferation and neuronal differentiation of newborn cells in the adult hippocampus in mice. *eNeuro*. 2018;5:e0067.
- Zanotti-Fregonara P, Lammertsma AA, Innis RB. Suggested pathway to assess radiation safety of <sup>18</sup>F-labeled PET tracers for first-in-human studies. *Eur J Nucl Med Mol Imaging*. 2013;40:1781–1783.